Effective Gating Charges per Channel in Voltage-dependent K^+ and Ca^{2+} Channels

FRANCESCA NOCETI,* PIETRO BALDELLI,‖ XIANGYANG WEI,‖ NING QIN,* LIGIA TORO,* LUTZ BIRNBAUMER,*§ and ENRICO STEFANI*‡

From the Department of *Anesthesiology, ‡Physiology, and §Biological Chemistry, School of Medicine, University of California, Los Angeles, Los Angeles, California 90095-1778; and ‖Department of Physiology, Baylor College of Medicine, Houston, Texas 77030

ABSTRACT In voltage-dependent ion channels, the gating of the channels is determined by the movement of the voltage sensor. This movement reflects the rearrangement of the protein in response to a voltage stimulus, and it can be thought of as a net displacement of elementary charges (e_0) through the membrane (z: effective number of elementary charges). In this paper, we measured z in *Shaker IR* (inactivation removed) K^+ channels, neuronal α_{1E} and α_{1A}, and cardiac α_{1C} Ca^{2+} channels using two methods: (*a*) limiting slope analysis of the conductance-voltage relationship and (*b*) variance analysis, to evaluate the number of active channels in a patch, combined with the measurement of charge movement in the same patch. We found that in *Shaker IR* K^+ channels the two methods agreed with a $z \simeq 13$. This suggests that all the channels that gate can open and that all the measured charge is coupled to pore opening in a strictly sequential kinetic model. For all Ca^{2+} channels the limiting slope method gave consistent results regardless of the presence or type of β subunit tested ($z = 8.6$). However, as seen with α_{1E}, the variance analysis gave different results depending on the β subunit used. α_{1E} and $\alpha_{1E}\beta_{1a}$ gave higher z values ($z = 14.77$ and $z = 15.13$, respectively) than $\alpha_{1E}\beta_{2a}$ ($z = 9.50$, which is similar to the limiting slope results). Both the β_{1a} and β_{2a} subunits, coexpressed with α_{1E} Ca^{2+} channels facilitated channel opening by shifting the activation curve to more negative potentials, but only the β_{2a} subunit increased the maximum open probability. The higher z using variance analysis in α_{1E} and $\alpha_{1E}\beta_{1a}$ can be explained by a set of charges not coupled to pore opening. This set of charges moves in transitions leading to nulls thus not contributing to the ionic current fluctuations but eliciting gating currents. Coexpression of the β_{2a} subunit would minimize the fraction of nulls leading to the correct estimation of the number of channels and z. Key words: charge movement • variance • noise fluctuations • limiting slope

INTRODUCTION

Hodgkin and Huxley (1952) first proposed that "changes in ionic permeability depend on the movement of some component of the membrane, which behaves as though it has a large charge or dipole moment . . . movement of any charged particle should contribute to the total current." This was the first proposition that the voltage sensor, a specific part of voltage-dependent channels, should rearrange itself with changes in the transmembrane electric field. Gating currents are the electrical manifestation of the voltage sensor rearrangement. The charge movement could either consist of a net displacement of unitary charges or be the result of local polarization of a cloud of charges or dipoles. Alternatively, charge movement could also arise from an asymmetric change in the electric field in relation to the voltage sensor, which encompasses changes in the overall structure of the protein, affecting the exposure of the charged residues to the external and internal sides of the membrane (Bezanilla and Stefani, 1994; Sigg et al., 1994; Sigworth, 1994; Larsson et al., 1996; Yang et al., 1996). At the time when Hodgkin and Huxley (1952) set the foundations for the theory of excitability, the primary structure of channel proteins was still unknown, but once channel proteins were cloned, the region for the voltage sensor was soon identified in the positively charged S4 transmembrane segment (Noda et al., 1984; Greenblatt et al., 1985; Guy and Seetharamulu, 1986; Catterall, 1988). Mutations of charged amino acids in the S4 segment of voltage-dependent channels affect the voltage sensitivity of channel opening (Stühmer et al., 1989; Liman et al., 1991; Papazian et al., 1991; Logothetis et al., 1992). Moreover, neutralization of S4-charged residues alters charge movement and the number of charges per channel (Perozo et al., 1994; Seoh et al., 1996). In agreement with the view that gating currents are the electrical manifestation of voltage-dependent conformational changes, it has been shown that some S4 residues have differential exposure to the cytoplasmic and extracellular environments depending on the membrane potential and that voltage-

Pietro Baldelli's current address is Department of Neuroscience, Università degli Studi, Torino 10125, Italy. Xiangyang Wei's current address is Institute of Molecular Medicine and Genetics and Department of Pharmacology and Toxicology, Medical College of Georgia, Augusta, Georgia 30912

Address correspondence to Dr. Enrico Stefani, UCLA, Department of Anesthesiology, BH-612 CHS, Box 951778, Los Angeles, CA 90095-1778. Fax: 310-825-6649; E-mail: estefani@anes.ucla.edu

dependent fluorescence changes are correlated to charge movement of S4 fluorophore-labeled residues (Yang and Horn, 1995; Larsson et al., 1996; Mannuzzu et al., 1996; Yang et al., 1996).

One critical quantity to evaluate in voltage-dependent channels is the size of the total charge movement per channel, detected as the number of effective charges per channel, z. z is the number of elementary charges, z_0, times the fraction of the field, x, that the charge traverses across the membrane ($z = z_0x$). z can be derived from the conductance to voltage (G-V) relationship by its limiting slope value at a very low probability of opening (Almers, 1978; Almers and Armstrong, 1980; Bezanilla and Stefani, 1994; Hirschberg et al., 1995). Using this method, Zagotta et al. (1994) found that z = 12–16 in *Shaker* K^+ channels. Alternatively, z can be obtained from the ratio between the limiting charge (Q_{max}) and the number of channels, which may be evaluated by the variance method in the same patch (Schoppa et al., 1992) or by channel particle measurement in freeze fractured membranes (Zampighi et al., 1995). In both cases, z was ≃13 in *Shaker* K^+ channels.

In this paper, we evaluated z in voltage-dependent channels expressed in *Xenopus laevis* oocytes. We expressed the K^+ channel *Shaker IR* (inactivation removed)[1] (Hoshi et al., 1990), the neuronal Ca^{2+} channels α_{1A} and α_{1E} (Starr et al., 1991; Schneider et al., 1994), and the cardiac Ca^{2+} channel α_{1C} (Wei et al., 1991). We measured charge movement and the number of channels in the same membrane patches by variance analysis, and we compared the z values obtained in this manner to the z values obtained by the limiting slope analysis. We improved the measurements in two ways: (*a*) for the variance analysis, we measured charge movement and ionic currents under the same ionic conditions and (*b*) we increased the resolution of G-V curves by using slow voltage ramps. For the α_{1E} Ca^{2+} channel, we evaluated the role of regulatory β subunits (Ruth et al., 1989; Perez-Reyes et al., 1992; Castellano et al., 1993*a*, 1993*b*) in determining z and the limiting open probability (Po_{max}) (Neely et al., 1993). We found that *Shaker IR* K^+ channels had $z \simeq 13$ with both methods. In the case of α_{1E} and $\alpha_{1E}\beta_1$ Ca^{2+} channels, we measured a larger z (≃14) using the variance analysis than by using the limiting slope method ($z \simeq 9$). However, when α_{1E} was coexpressed with the regulatory β_{2a} subunit, which increased Po_{max}, both methods gave consistent z values of ≃9. The other Ca^{2+} channels tested (α_{1A} and α_{1C}) had $z \simeq 9$ with the limiting slope method. The constraints given by these results to a kinetic model of channel function are discussed.

[1]*Abbreviations used in this paper*: HP, holding potential; *IR*, inactivation removed; LSA, limiting slope analysis; SHP, subtracting holding potential.

MATERIALS AND METHODS

Molecular Biology and Oocyte Injection

We used cDNA encoding *Shaker* H4 K^+ channel, which is nearly identical to the *Shaker B* clone (Tempel et al., 1987; Kamb et al., 1988). We used the deletion Δ6-46 (*Sh*H4-*IR*) (Hoshi et al., 1990) which does not inactivate. RNA was synthesized from each cDNA construct by linearization of the pBluescript plasmids (Stratagene Inc., Madison, WI) with EcoRI and transcription with T7 RNA polymerase (Promega Corp., La Jolla, CA) using mMessage mMachine™ (Ambion Inc., Austin, TX). 50 nl of cRNA at 0.2–1.0 μg/μl concentration was injected into mature *Xenopus laevis* oocytes. The oocytes were kept at 18°C for 1–2 d before the experiments.

For Ca^{2+} channels, the neuronal α_{1E} and α_{1A} subunits, the cardiac α_{1C} (Schneider et al., 1994; Starr et al., 1991; Wei et al., 1991), and the β subunits β_{1a}, β_{1b}, and β_{2a} (Ruth et al., 1989; Castellano et al., 1993*a*, 1993*b*; Perez-Reyes et al., 1992) were expressed in *Xenopus laevis* oocytes. The carboxyl terminal (α_{1Cdel2}) and the amino terminal (ΔN60) deletion mutants (Wei et al., 1994*a*; 1994*b*) of the cardiac α_{1C} clone were used. ΔN60 can express large Ca^{2+} currents with properties similar to the full length clone α_{1C}. This amino-terminal deletion will be referred to as α_{1C}. The plasmids containing cDNA fragments encoding the α_1 and β subunits were digested with HindIII. The linearized templates were treated with 2 μg proteinase K and 0.5% SDS at 37°C for 30 min, then twice extracted with phenol/chloroform, precipitated with ethanol, and resuspended in distilled water to a final concentration of 0.5 μg/μl. The cRNAs were transcribed from 0.5 μg of linearized DNA template at 37°C with 10 U of T7 RNA polymerase (Boehringer Mannheim Biochemicals, Indianapolis, IN), in a volume of 25 μl containing 40 mM Tris-HCl, pH 7.2, 6 mM $MgCl_2$, 10 mM dithiothreitol, 0.4 mM each of ATP, GTP, CTP, and UTP, 0.8 mM $m^7G(5')PPP(5')GTP$. The transcription products were extracted with phenol and chloroform, twice precipitated with ethanol and resuspended in double distilled water to a final concentration of 0.2 μg/μl, and 50 nl were injected per oocyte. For both Ca^{2+} and K^+ channels, the oocytes were defolliculated, before injection, by collagenase treatment (type I, 2 mg/ml for 40 min at room temperature; Sigma Chemical Co., St. Louis, MO). Oocytes were maintained at 19°C in Barth solution. Recordings were done 4–12 d after RNA injection.

Electrophysiology

The patch technique (10–30 μm pipette diameter) in cell attached configuration was used for the variance analysis (Hilgemann, 1989). Solutions for *Shaker IR* experiments were: bath solution in mM, K-methanesulfonate 110, HEPES 10, $MgCl_2$ 2, EGTA 0.1 (KMES), and pipette solution in mM, K-methanesulfonate 110, HEPES 10, $CaCl_2$ 2, (KMESCa2). The Cs^+ solutions were like the K^+ solutions with Cs-methanesulfonate (CsMES and CsMESCa2) instead of K-methanesulfonate. The oocytes viteline membrane was mechanically removed in KMES, thereafter, the oocyte membrane was mechanically permeabilized by local damage for solution equilibration. For Ca^{2+} channels we used the same bath solution (KMES), whereas the pipette solution contained in mM, $Bamethanesulfonate_2$ 75, $BaCl_2$ 5, HEPES 10 (BaMES 75). The experiments for the limiting slope analysis in Ca^{2+} channels were performed using the cut-open oocyte technique (COVG; Stefani et al., 1994). Microelectrode solution was: Na-methanesulfonate 2.7 M, Na_2-EGTA 10 mM, NaCl 10 mM. External solutions were in mM: $Ba\text{-}methanesulfonate_2$ 10, Na-methanesulfonate 96, HEPES 10 (BaMES 10) and BaMES 75. All solutions were buffered to pH 7.0. The oocyte membrane exposed to the bottom chamber was permeabilized with 0.1% saponin in the internal sa-

line (K-glutamate 110 mM, HEPES 10 mM). Before the experiments, 100 nl of 50 mM Na_4-BAPTA (1,2-bis(*o*-aminophenoxy)-ethane-*N,N,N',N'*-tetraacetate) was injected into the oocytes, to prevent contaminant Ba^{2+}-activated Cl^- currents (Neely et al., 1994).

The oocyte membrane was stimulated with voltage ramps from holding potentials of −90 and −120 mV. Currents were filtered at one-fifth of the sampling frequency. Slow voltage ramps were used to reach quasi steady state. An experimental test for the adequacy of the voltage ramps was the use of a triangle wave which elicited a symmetrical current response. In general, ramps to voltages near ionic current detection were slow enough to reach steady state; however, for larger depolarizations they could induce significant channel inactivation. Compensation for linear capacitative and resistive current was performed. Control oocytes did not show any nonlinear response to the voltage ramps. During voltage ramp stimulation, the presence of nonlinear capacitative currents, such as gating currents, should induce nonlinear outward currents. This component was undetectable in our recording conditions, in part due to the slow speed of the ramp, and should not induce systematic errors in the evaluation of the limiting slope.

Experiments were performed at room temperature (22–23°C) for K^+ channels and at room temperature (22–23°C) and 30°C for Ca^{2+} channels.

Data Analysis

Variance analysis. Series of identical records were recorded pulsing to a positive potential from the holding potential. Pairs of M subsequent records $X_i(t)$, $X_{i+1}(t)$ were subtracted in order to compute the experimental non-stationary variance as:

$$\sigma^2(t) = \frac{2}{M-1}\sum_{i=1}^{M-1}[Y_i(t) - \mu_i]^2,$$

where $Y_i(t)$ was

$$Y_i(t) = \frac{1}{2}[X_i(t) - X_{i+1}(t)],$$

and μ_i was the mean value of $Y_i(t)$. The average basal variance at the holding potential was subtracted from the variance during the pulse stimulation. The subtracted variance was plotted vs. the mean current $I(t)$ (average of the records) and fitted to the theoretical variance function with the assumption that the single channel current has only one non-zero value (Begenisich and Stevens, 1975; Sigworth, 1980; Conti et al., 1984):

$$\sigma^2(t) = I(t)\,i - \frac{I(t)^2}{N}, \qquad (1)$$

where i is the single channel current amplitude, and N is the number of channels. i was obtained from the initial slope of the variance ($t = 0$), and N was determined by the abscissa of the maximum of the parabolic function (corresponding to open probability $Po = 0.5$), according to the first derivative of the variance:

$$\frac{\partial\sigma^2(t)}{\partial I(t)} = i - \frac{2}{N}I(t).$$

The maximum open probability, Po_{max}, was extrapolated from the maximum mean current I_{max},

$$Po_{max} = \frac{I_{max}}{iN},$$

and the effective charge per channel, z, was extrapolated from the maximum charge Q_{max} (time integral of the gating current at saturating potential),

$$z = \frac{Q_{max}}{e_0 N}.$$

Limiting slope analysis (LSA). The ionic current recorded during a voltage ramp was subtracted off line from linear leakage and subsequently converted into conductance by dividing the ionic current by its driving force. The leakage subtraction was performed by fitting the leak current to a straight line before the detection of the inward ionic current and by subsequently subtracting this linear component from the total current. Current data points recorded at potentials more negative than −80 mV and of −65 mV were fitted for the linear leakage in the experiments shown for the *Shaker IR* K^+ channel and $\alpha_{1C}\beta_{2a}$ Ca^{2+} channel, respectively (see Figs. 4 and 9). Under our experimental conditions, the large inward K^+ and Ca^{2+} currents were easily distinguishable from the linear leak current. The conductance vs. potential (*G-V*) plot was fitted to the monoexponential approximation of the Boltzmann function in the limit for very negative potentials,

$$G(V) = Ae^{\frac{e_0 V}{zkT}}, \qquad (2)$$

where $G(V)$ is the conductance (in S), z the number of effective charges per channel, e_0 the electronic charge (1.602×10^{-19}C), k the Boltzmann constant (1.38×10^{-23}J/K), T the absolute temperature (in K), V the membrane potential (in V), and A the amplitude of the exponential (in S). This approximation was resolved for a linear sequential model with one open state (Almers, 1978; Almers and Armstrong, 1980).

The z value evaluated from the fit to Eq. 2 was then compared with the slope of the ln$G$ vs. conductance (see APPENDIX):

$$z(V) = \frac{kT}{e_0}\frac{\mathrm{d}}{\mathrm{d}V}\ln G(V) \qquad (3)$$

All data are expressed as mean ± SEM with the number of observations (n) in parentheses.

RESULTS

Effective Number of Charges per Channel in the Shaker IR K^+ Channel

Variance analysis in isotonic K^+. Variance experiments have been performed on *Shaker IR* K^+ channels in order to extract the value of z. Schoppa et al. (1992) performed the first measurements of z in excised patches. The number of channels, N, in the patch was obtained from nonstationary noise analysis of ionic currents, and thereafter, the charge in the same patch was measured after blocking the ionic currents by adding internal tetraethylammonium (TEA). Since it is well established that internal TEA greatly slows down charge return for depolarizing pulses that open the channel (Bezanilla et al., 1991; Perozo et al., 1993), we decided to measure charge per channel in the absence of ion channel blockers. We performed the experiments in isotonic K^+ solutions, and in mechanically permeabilized oocytes in order to equilibrate the intracellular and extracellular K^+ concentrations. Under these conditions, charge movement could be measured at the K^+ reversal potential (close to 0 mV) using pulses from holding potentials of −90 and −120 mV; these pulse protocols should be able to displace most of the charge. Experiments were performed in the cell-attached mode to prevent run down of the currents. This method allowed

us to bracket measurements of charge movement and N. A potential complicating factor in these measurements is the induction of a slow inactivation process during the repetitive stimulation for the variance analysis. This process may lead to an underestimation of N due to the presence of silent traces. Since slow inactivated channels can displace a normal amount of charge (Olcese et al., 1996), the underestimation of N will lead to an overestimation of the number of effective charges per channel. In view of this, we measured N at different stimulating frequencies. We decided to use frequencies that did not change N, and thus, did not induce the slow inactivation process. Typically, we used 5–8-ms pulses to +20 mV every 0.5–1 s, which induced K^+ currents with constant amplitude.

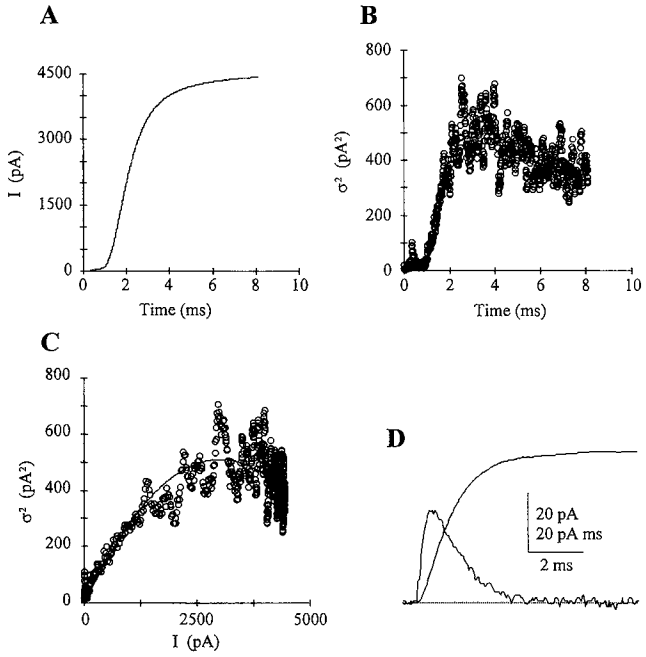

FIGURE 1. Variance analysis in *Shaker IR* K^+ channel in KMES. (*A*) Mean current from 100 traces recorded with the patch technique (cell attached configuration) in an oocyte injected with *Shaker IR* K^+ channel cRNA. Holding potential (HP) −90 mV and pulses to +20 mV. Linear subtraction with P/4 from subtracting holding potential (SHP) −90 mV. (*B*) Variance vs. time plot; the experimental variance was calculated subtracting sequential pairs of the 100 records (see METHODS). (*C*) Variance-mean plot (○) and fit (*solid line*) to the theoretical variance function $\sigma^2 = Ii - \frac{I^2}{N}$. The parameters i and N (single channel current and number of channels, respectively) were: $i = 0.34$ pA and $N = 1.78 \times 10^4$. The maximum open probability (Po_{max}), calculated from the maximum mean current value, was 0.73. (*D*) Gating current and its time integral from the same patch. The gating current was recorded pulsing to the K^+ reversal potential. HP −120 mV, pulse to 0 mV. P/4 subtracting pulses from SHP −120 mV. The maximum value of the charge (Q_{max}) was 41.8 fC (average of five records). The effective charge per channel $\left(z = \frac{Q_{max}}{e_0 N}\right)$ calculated from this experiment was $z = 14.6$. External solution KMES; pipette solution KMESCa2. Temperature 22°C.

Fig. 1 shows variance analysis and charge movement in isotonic KMES (external and pipette solution). Fig. 1, *A* and *B* shows the time course of the average current for a +20 mV pulse and the corresponding variance. The noise fluctuations in *B* have, as expected, a biphasic time course correlating to the channel open probability, Po, during the activation of the ionic current. The variance-mean current plot in Fig. 1 *C* has been fitted to Eq. 1 (see MATERIALS AND METHODS). The fitted parameters for this experiment were $i = 0.34$ pA and $N = 1.78 \times 10^4$ channels. The maximum open probability (Po_{max}) inferred from the maximum value of the mean ionic current (I_{max}) was 0.73. From the integral of the gating current in the same patch (Fig. 1 *D*), we obtained a value of $z = 14.6$.

Variance analysis in isotonic Cs^+. The experiments in isotonic KMES were critically dependent on the adequate measurement of charge movement at the K^+ reversal potential. To increase our resolution in this determination, we performed equivalent experiments in isotonic CsMES in mechanically permeabilized oocytes. Under these conditions, we expected much smaller ionic currents, due to changes in the single channel amplitude, which would facilitate charge movement measurements (Heginbotham and MacKinnon, 1993). For these measurements, we used big size patch pipettes (~10–30 μm) to record larger ionic and gating currents from a much larger number of channels. The series of ionic currents at different stimulation pulses in Fig. 2 *A* illustrates large gating currents preceding the ionic currents. Fig. 2, *B* and *C* show the isolation of the gating current from the ionic current by pulsing to the Cs^+ reversal potential (2 mV), together with the time integral of the gating current (total charge). To obtain the number of channels in the same patch, we performed the procedures illustrated in Fig. 3. Panels *A* and *B* show the time course of the mean current and the variance, respectively. Noise fluctuations were analyzed both in the activation and deactivation of the ionic current. The first increase in the noise fluctuations corresponds to the activation process, while the late increase correlates with deactivation (decay of the inward tail current). The two plots of the experimental variance vs. mean current (Fig. 3, *C* and *D*) were simultaneously fitted to the theoretical variance with a constant number of channels for the two fits. We obtained $N = 13.7 \times 10^4$ channels with Po_{max} of ~0.75, for both the activation and deactivation. The value of z inferred with this procedure was 13.49.

As illustrated by the records in Fig. 3 *A*, in isotonic CsMES, the ionic currents at the beginning (ON) and the end (OFF) of the pulse can be contaminated by the associated gating currents. Since noise fluctuations of

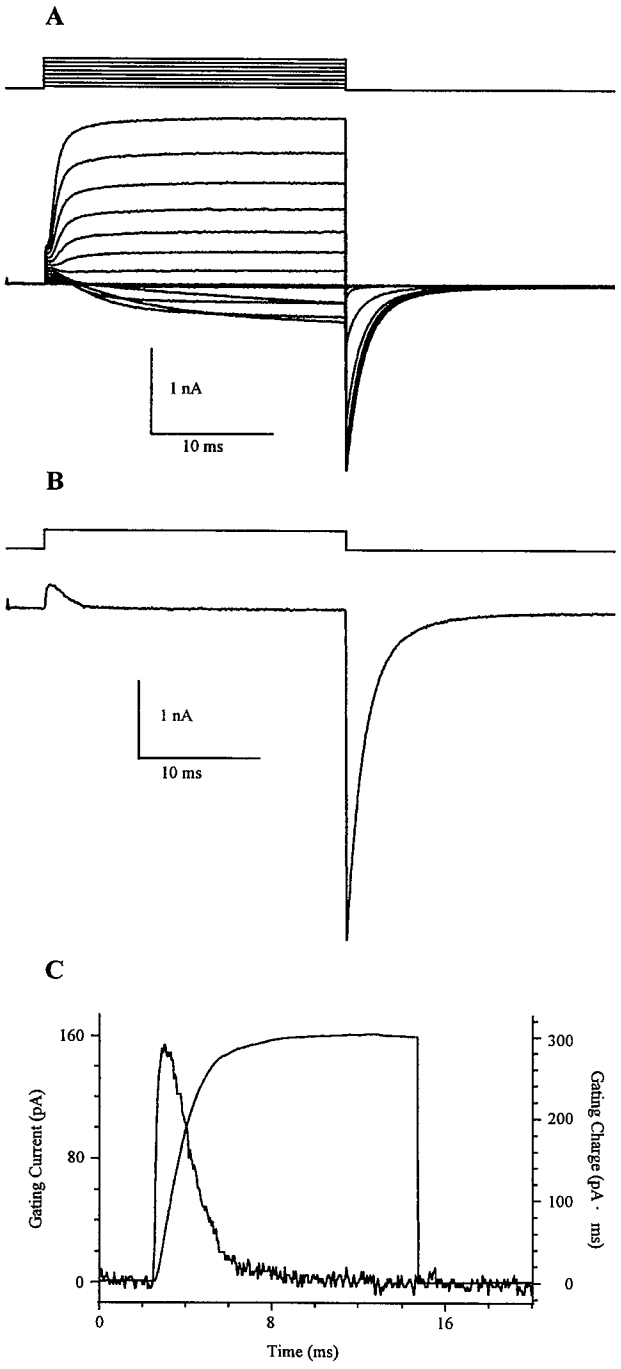

FIGURE 2. Ionic and gating currents in *Shaker IR* K^+ channel in CsMES. (*A*) Ionic current traces recorded with the patch technique from an oocyte incubated in 110 CsMES (cell attached configuration) after mechanical permeabilization. Pipette solution: CsMESCa2; temperature 22°C. HP −90 mV and 25-ms pulses to +70 mV in 10-mV increments. P/4 subtracting pulses from SHP −90 mV. (*B*) Gating current in the same patch with pulses to 2 mV from HP −90 mV. P/4 from SHP −90 mV. (*C*) Gating currents at higher gain with its time integral. Q_{max} = 297 fC.

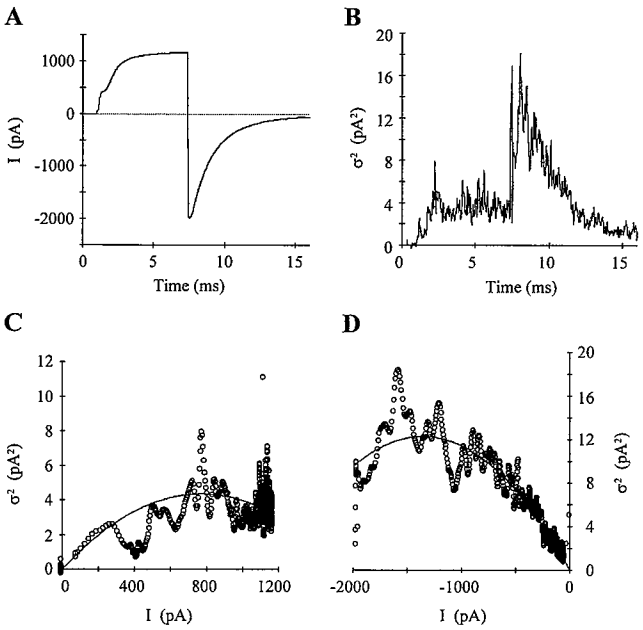

FIGURE 3. Variance analysis in *Shaker IR* K^+ channel in CsMES. Same patch as in Fig. 2. 100 subsequent records were averaged, and sequential pairs of records were subtracted to calculate the variance parameters. (*A*) Mean current vs. time; the trace shown here is the average of 100 current records. HP −90 mV and the pulse voltage +50 mV. (*B*) Variance time plot of the activation and the deactivation current phases. (*C* and *D*) Variance-mean current plots from the activation (*C*) and deactivation (*D*) phases of the current. The experimental variance points in *C* and *D* (○) have been simultaneously fitted to the theoretical variance function in order to attain the values of i and N. $i_{activation}$ = 0.011 pA, $i_{deactivation}$ = 0.019 pA, $N = 13.7 \times 10^4$. Po_{max} was about 0.75. The charge per channel was calculated as in Fig. 1, using the Q_{max} value of the integral of the gating current shown in Fig. 2 *C*; z = 13.49.

gating currents are several orders of magnitude smaller than noise fluctuations of ionic currents, they should not have affected our calculation (Sigg et al., 1994). Nevertheless, the mean current after the pulse jump could be overestimated by the associated gating currents. This overestimation is more significant in the ON than in the OFF, due to the relative size of gating and ionic currents. Gating current contamination should be negligible for *Po* values >0.5 for the ON and <0.5 for the OFF, which are the critical regions for the parabolic fit. The reliability of our calculations, however, was confirmed by the consistent single channel conductance (0.2 pS in ON and OFF) and *Po* (0.75 ON and 0.76 OFF) values obtained from ON and OFF pulses.

Limiting slope analysis of the conductance-voltage (G-V) curve. A classical way to calculate z is by fitting the initial phase of the *G-V* curve to a single exponential as in Eq. 2 (see MATERIALS AND METHODS). We have used this approach in the *Shaker IR* K^+ channel and obtained similar results as previously shown with the variance analysis. To increase the voltage resolution, we used

slow ramp stimulation (3.5 mV/s from −90 to −20 mV). This ramp is adequate to obtain a quasi steady state *G-V* relationship at potentials more negative than −60 mV. However, for larger depolarizations, conductance values are slightly underestimated due to the induction of slow inactivation during the ramp. The steady state of the *G-V* curve at potentials more negative than −60 mV was confirmed by varying the speed of the ramp and by testing the symmetry of the current response to a symmetric triangle wave. Fig. 4 *A* shows the ionic current flowing through the channels in response to a voltage ramp from −90 to −20 mV. Fig. 4 *B* is the corresponding conductance which was fitted to Eq. 2 for very negative potentials (−80 to −65 mV) to approximate to the limit $Po \rightarrow 0$. The semilog plot of the *G-V* curve (Fig. 4 *C*) tended to a straight line when the membrane potential was less than −65 mV; the evaluated parameters of the fit were z = 12.76 and A = 1.17×10^{17} pS. To verify the validity of our assumption we calculated $z(V)$ at different voltages using Eq. 3 (see MATERIALS AND METHODS), and plotted $z(V)$ as a function of the corresponding conductance to obtain a $z(V)$ vs. $G(V)$ curve. Fig. 4 *D* confirms that $z(V)$ approaches a limiting value close to the fitted value of z (straight line). Similar z values were obtained from *G-V* curves derived during pulse stimulation. *G-V* curves from peak tail measurements gave smaller z values, since they were significantly contaminated by OFF gating currents at negative potentials.

Fig. 5 shows a summary of the results for *Shaker IR*. The values of the total charge Q_{max} (integral of the gating current) are plotted here as a function of the number of channels (A). The slope of the regression line to

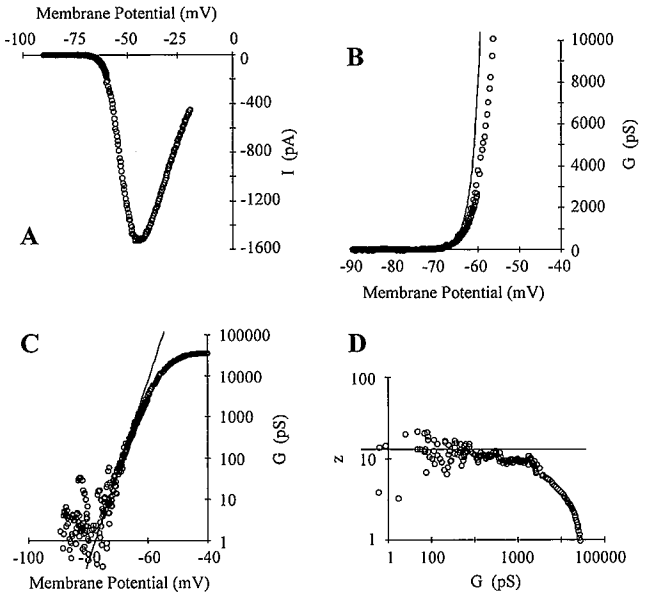

FIGURE 4. Limiting slope analysis in *Shaker IR* K^+ channel. (*A*) Ionic current recorded with the patch technique in the cell attached configuration. HP −90 mV. Slow depolarization (0.0035 mV/ms) with a voltage ramp from −90 to −20 mV. Linear leakage correction was performed off line using a linear fit to the points at potentials more negative than −80 mV. Data points were decimated (average of five points). (*B*) *G-V* relationship (○), in a linear plot, at potentials near detection of current activation. Data points between −80 and −65 mV were fitted to $Ae^{\frac{z_a V}{kT}}$ (*solid line*). The fitted parameters were $A = 1.17 \times 10^{17}$ pS and z = 12.76. (*C*) *G-V* curve (○) and fitted limiting slope (*solid line*) in semilog scale. (*D*) Relationship between the calculated z (○) at different potentials and the corresponding conductance. z values were calculated as $z = \frac{kT}{e_o}\frac{\mathrm{d}}{\mathrm{d}V}\ln G$. The voltage derivative of $\ln G$ was obtained from age running slope of 20 data points. The straight line shows the fitted value of z. External solution KMES; pipette solution KMESCa2. Temperature 22°C.

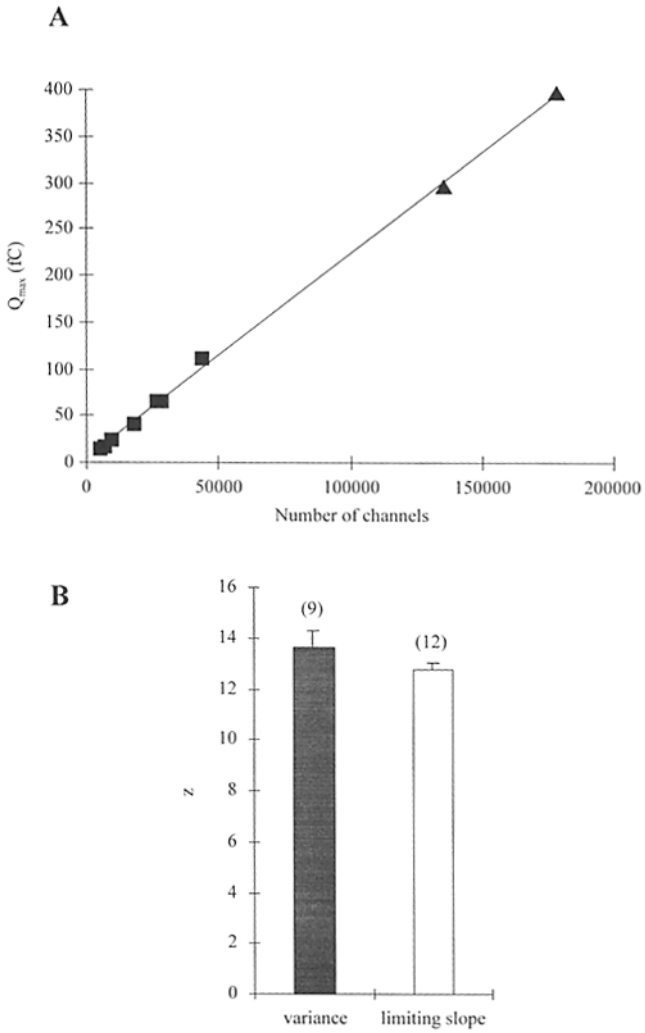

FIGURE 5. Charges per channel calculated from the variance analysis and limiting slope methods in *Shaker IR* K^+ channel. (*A*) Q_{max}-N relationship fitted to a straight line. The slope gives the effective number of charges per channel. ■, experiments in KMES; ▲, experiments in CsMES. (*B*) Summary plot of z values. $z_{variance}$ = 13.62 ± 0.63 (n = 9) and $z_{limiting\ slope}$ = 12.79 ± 0.26 (n = 12). Data are slope ± SEM with n the number of observations.

the experimental points gives the measure of the effective number of charges per channel from the variance experiments. The slope from nine experiments (including the two CsMES experiments, ▲) was 0.00218 pA·ms, which corresponds to a $z_{variance}$ of 13.62 ± 0.63. Similarly, the average of the limiting slope results gave a $z_{limiting\ slope}$ of 12.79 ± 0.26. The bar graph (*B*) compares both methods. We can conclude that both types of measurements give similar values of *z*, which are close to 13.

Effective Number of Charges per Channel in Ca^{2+} Channels

We investigated the number of charges per channel in expressed cloned neuronal (α_{1A}, α_{1E}) and cardiac (α_{1C}) channels, and the potential effect of the auxiliary β subunits (β_{2a}, β_{1a}, β_{1b}) on *z* and Po_{max}. In previous work, it has been demonstrated that the β subunits facilitate Ca^{2+} channel opening at the single channel level and that they shift the *G-V* curve of macroscopic currents towards more negative potentials (Singer et al., 1991; Williams et al., 1992; Neely et al., 1993; Costantin et al., 1995; Neely et al., 1995). The facilitation occurs without detectable changes in charge movement kinetics (Neely et al., 1993; Olcese et al., 1994).

Variance analysis in α_{1E} Ca^{2+} channels: effect of β subunits on Po_{max} and z values. The measurements were performed in large patches (15–20 μm) in the cell attached mode. Oocytes were bathed in KMES, and BaMES 75 was used in the pipette. One difficulty in calculating *N* for Ca^{2+} channels from variance-mean plots is to achieve a high enough *Po* (0.5) to adequately estimate the curvature of the parabola. Therefore, to obtain the limiting *Po* value, we increased the bath temperature to 30°C, and we stimulated the bath with pulses to 150 mV every 0.6 s. This pulse protocol did not induce inactivation since peak tail currents remained constant.

Fig. 6 illustrates the procedures to obtain *N* and the Po_{max} for the neuronal Ca^{2+} channel α_{1E} alone and coexpressed with β subunits (β_{1a} and β_{2a}). The typical ionic current response to a +150 mV voltage step (from a holding potential of −80 mV) followed by a repolarization to −30 mV is shown in Fig. 6 *A*, while the traces in *B* show sequentially subtracted tail currents recorded during the jump to −30 mV. It can be noted that the fluctuations are small immediately after the termination of the pulse to +150 mV, peak ~1 ms after the pulse, and then slowly decay to a basal value. The variance is shown together with the mean current in *C*. The three graphs in *E*, *F*, and *G* show plots and fits of the variance vs. mean current for α_{1E}, $\alpha_{1E}\beta_{1a}$, and $\alpha_{1E}\beta_{2a}$. The Po_{max} reached by both α_{1E} and $\alpha_{1E}\beta_{1a}$ was low (0.55 and 0.61, respectively), while in the case of $\alpha_{1E}\beta_{2a}$ Po_{max} was 0.84. As was the case for K^+ channels, gating currents could induce errors in the estimation of the ionic current at the beginning of a voltage jump.

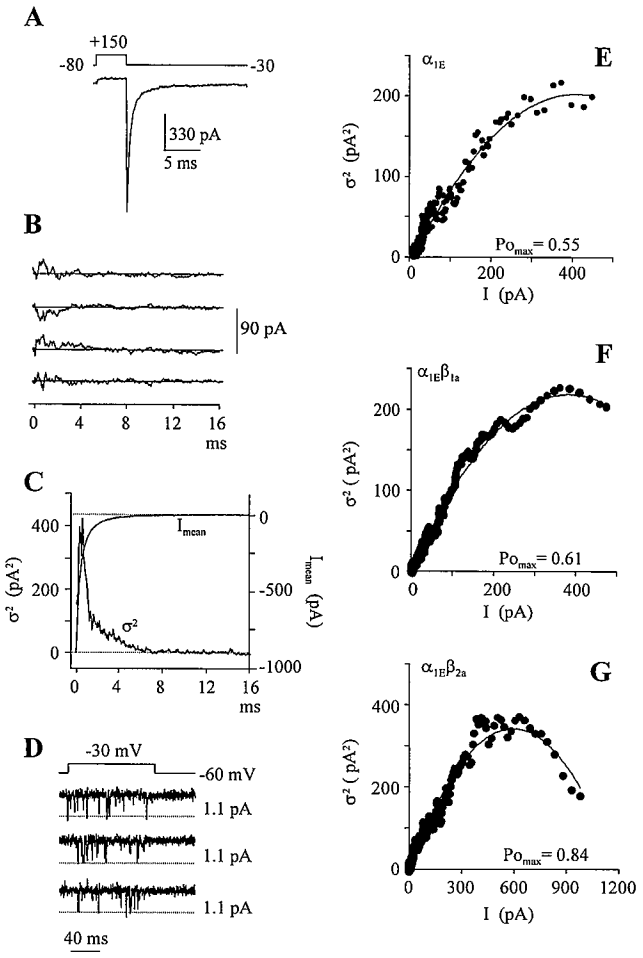

FIGURE 6. Variance analysis experiments in Ca^{2+} channels (α_{1E} and auxiliary regulatory subunits β_{1a} and β_{2a}). (*A*) Current recorded in an oocyte coexpressing the neuronal α_{1E} Ca^{2+} channel and the β_{2a} subunit. The experiment was performed in the cell attached configuration of the patch technique. External solution KMES; pipette solution BaMES 75. Temperature 30°C. HP −80 mV, pulse to 150 mV followed by a return potential to −30 mV. (*B*) Sequentially subtracted tail currents vs. time. (*C*) Mean tail current and the corresponding non-stationary variance. (*D*) Single channels recorded at −30 mV under the same ionic conditions in the same oocyte. (*E*, *F*, and *G*) Variance-mean data and corresponding fitted curves to the theoretical function in α_{1E}, $\alpha_{1E}\beta_{1a}$, and $\alpha_{1E}\beta_{2a}$. The fitted parameters and calculated Po_{max} were: i = 1.00 pA, N = 801, Po_{max} = 0.55 in α_{1E} expressed alone; i = 1.13 pA, N = 674, Po_{max} = 0.61 in $\alpha_{1E}\beta_{1a}$ and i = 1.14 pA, N = 1033, Po_{max} = 0.84 in $\alpha_{1E}\beta_{2a}$.

Hypothetical gating current noise should be negligible in respect to the ionic current noise (Sigg et al., 1994), and the negative pulses to −30 mV elicit large ionic tail currents (~1 nA) as compared to gating current amplitude (50–60 pA). Our measurements were validated by the correspondence between single channel amplitude at −30 mV recorded with small pipettes (≃1 pA, *D*), and the calculated values from the initial slope of the variance-mean curves ($i_{\alpha 1E}$ = 1.0 pA, $i_{\alpha 1E\beta 1a}$ = 1.13 pA, $i_{\alpha 1E\beta 2a}$ = 1.14 pA). The traces in Fig. 6 *D* were recorded

at 2 kHz and sampled at 100 μs per point, which was sufficient to resolve the single channel openings. For the variance analysis, traces were collected at 10 kHz and sampled at 20 μs per point. Thus, the variance analysis should provide an adequate bandwidth to resolve the amplitude of the unitary events. This was confirmed by performing variance analysis by filtering up to 2 kHz, which gave similar results.

Fig. 7 illustrates Ca^{2+} currents recorded with macropatches (*A*). The bar plot in *B* represents a summary of the Po_{max} results for the α_{1E} Ca^{2+} channel with or without β subunits. Po_{max} for $\alpha_{1E}\beta_{2a}$ was significantly different from both α_{1E} and $\alpha_{1E}\beta_{1a}$ ($P < 0.001$ and $P < 0.005$, respectively). In the voltage activation curves of Fig. 7 *C*, absolute *Po* values were obtained from peak tail currents (normalized to the limiting *Po* value obtained from the variance-mean plots). Both β subunits shift the activation curve toward more negative potentials, while only the β_{2a} subunit increases the Po_{max} value.

The total charge Q_{max} was measured in the α_{1E} Ca^{2+} channel by the same procedure previously illustrated for the *Shaker IR* K^+ channel. Gating currents were recorded at a voltage close to the reversal potential in the same patch where the traces for the variance analysis had been collected. The maximum values of the integrals of the gating currents (Fig. 8, *A* and *B* show records from an $\alpha_{1E}\beta_{1a}$ experiment) were then plotted vs. the number of channels. Fig. 8 *C* shows the results for α_{1E}, $\alpha_{1E\beta 1a}$, and $\alpha_{1E}\beta_{2a}$. The slope of the regression lines for α_{1E} (▲) and $\alpha_{1E}\beta_{1a}$ (■) data points are: 0.00237 pA·ms and 0.00242 pA·ms, corresponding to $z_{\alpha 1E} = 14.77 \pm 0.29$ and $z_{\alpha 1E\beta 1a} = 15.13 \pm 0.71$. These values are not significantly different (P = 0.63). In the case of $\alpha_{1E}\beta_{2a}$ the slope of the regression line to the data points (△) was 0.00152 pA·ms, corresponding to $z_{\alpha 1E\beta 2a} = 9.50 \pm 0.14$. This *z* value was significantly different from the *z* values for α_{1E} and $\alpha_{1E}\beta_{1a}$ ($P < 0.01$ in both cases).

Limiting slope analysis of the G-V curve. Fig. 9 illustrates a limiting slope experiment in $\alpha_{1C}\beta_{2a}$ performed with the

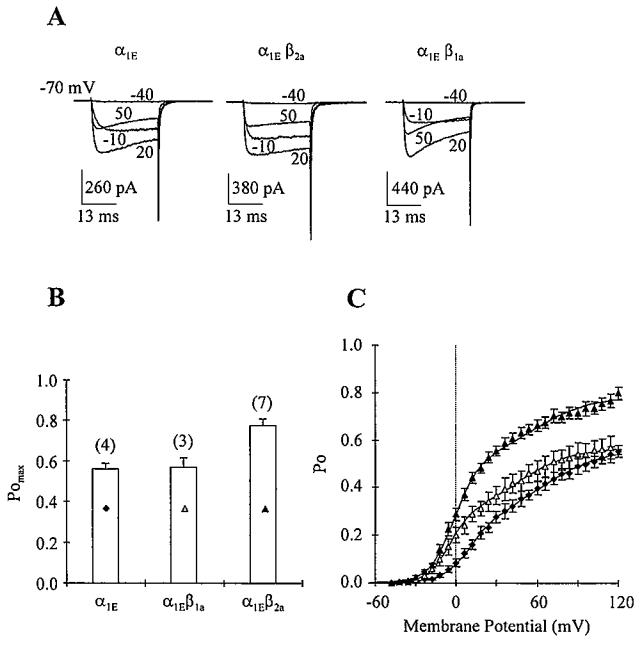

FIGURE 7. Po_{max} and *Po*-voltage curves in Ca^{2+} channels. (*A*) Representative records of Ca^{2+} currents in cell attached mode. (*B*) Summary plots of Po_{max} for the neuronal α_{1E} Ca^{2+} channel in the presence and absence of β subunits. $Po_{max} = 0.56 \pm 0.026$ in α_{1E} ($n = 4$), $Po_{max} = 0.57 \pm 0.045$ in $\alpha_{1E}\beta_{1a}$ ($n = 3$) and $Po_{max} = 0.78 \pm 0.029$ in $\alpha_{1E}\beta_{2a}$ ($n = 7$). (*C*) *Po*-voltage curves obtained from the Po_{max} values for the α_{1E} (◆), $\alpha_{1E}\beta_{1a}$ (△) and $\alpha_{1E}\beta_{2a}$ (▲) Ca^{2+} channels. Values are mean ± SEM (n = number of observations). External solution KMES; pipette solution BaMES 75. Temperature 30°C.

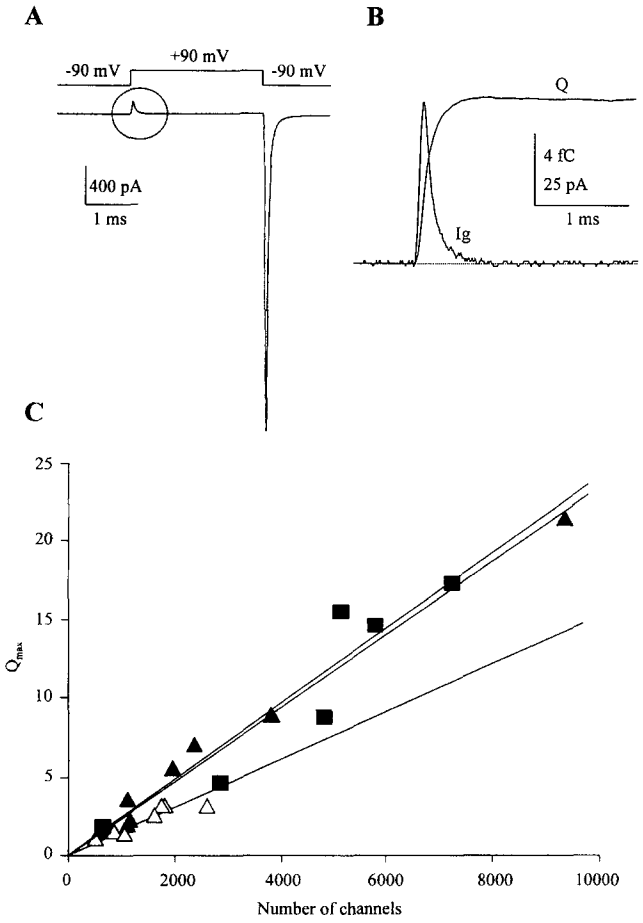

FIGURE 8. Evaluation of the number of effective charges per channel, *z*, from the variance analysis in Ca^{2+} channels (α_{1E}, $\alpha_{1E}\beta_{1a}$, and $\alpha_{1E}\beta_{2a}$). (*A*) Gating currents in $\alpha_{1E}\beta_{1a}$ Ca^{2+} channel. HP −90 mV, pulsed to the reversal potential (+90 mV). (*B*) ON gating current and its time integral. $Q_{max} = 8.5$ fC, $N = 3300$ as evaluated from the corresponding variance fit; $z = 15.8$. (*C*) Q_{max}-*N* plot in α_{1E}, (▲), $\alpha_{1E}\beta_{1a}$, (■) and $\alpha_{1E}\beta_{2a}$, (△). Fitted slopes of the three straight lines to the experimental data give the number of effective charges per channel: $z = 14.77 \pm 0.29$ in α_{1E} ($n = 7$); $z = 15.13 \pm 0.71$ in $\alpha_{1E}\beta_{1a}$ ($n = 7$), $z = 9.50 \pm 0.14$ in $\alpha_{1E}\beta_{2a}$ ($n = 8$). Values are the slope ± SEM (n = number of observations). External solution KMES; pipette solution BaMES 75. Temperature 30°C.

same strategy as the experiment shown in Fig. 4 for *Shaker IR*. The experiments were performed with the COVG technique with external BaMES 10. A slow voltage ramp from −90 to −20 mV (3.5 mV/s) was used to elicit the ionic current in Fig. 9 *A*, which was then converted into conductance (Fig. 9, *B* and *C*). The monoexponential fit to the initial part of the *G-V* curve (−80 to −50 mV) gave $A = 3.63 \times 10^6$ nS and $z = 7.20$.

Limiting slope experiments were also performed with the COVG technique in the presence of external BaMES 75. Under these ionic conditions, a shift to more positive potentials of ~20 mV in the activation curves was observed, which can be explained by changes in the surface potential. This shift did not induce any change in the effective charge moved.

Fig. 10 summarizes the number of charges obtained with the two methods for different Ca^{2+} channels and β subunits. Both methods agreed for the $\alpha_{1E}\beta_{2a}$ combination, however, the variance method gave larger z values for α_{1E} and $\alpha_{1E}\beta_1$. This discrepancy may be explained by the correlation between a low value of the Po_{max} in α_{1E} and $\alpha_{1E}\beta_{1a}$ with more occurrence of traces without opening ("nulls"). Null traces will have charge movement but will not contribute to the variance, causing an underestimation of N. The limiting slope method gave similar results, for all Ca^{2+} channel combinations tested, of ~9 e_0.

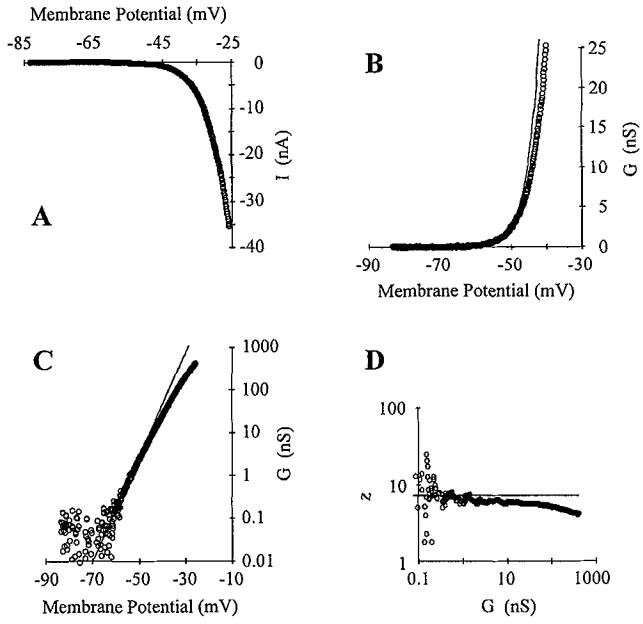

FIGURE 9. Limiting slope analysis in $\alpha_{1C}\beta_{2a}$ Ca^{2+} channel. (*A*) Ionic current recorded with the cut-open oocyte technique (COVG) from an oocyte expressing the $\alpha_{1C}\beta_{2a}$ Ca^{2+} channel. The external solution was BaMES 10. HP −90 mV. Slow depolarization (0.0035 mV/ms) with a voltage ramp to −20 mV. Linear leakage correction was performed off line using a linear fit to the points at potentials more negative than −65 mV. Data points were decimated (average of three points). (*B*) *G-V* relationship (○), in a linear plot, at potentials near detection of current activation. Data points between −80 and −50 mV were fitted to $Ae^{\frac{z e_0 V}{kT}}$ (*solid line*). The fitted parameters were $A = 3.63 \times 10^6$ nS and $z = 7.20$. (*C*) *G-V* curve (○) and fitted limiting slope (*solid line*) in semilog scale. (*D*) Relationship between the calculated z (○) at different potentials and the corresponding conductance. z values were calculated as $z = \frac{kT}{e_0}\frac{d}{dV}\ln G$. The voltage derivative of lnG was obtained from an average running slope of 20 data points. The straight line shows the fitted value of z. External solution BaMES 10; room temperature.

DISCUSSION

The salient findings of this work are: (*a*) The movement of the voltage sensor in *Shaker IR* K^+ channels can be evaluated through variance and limiting slope analysis. The results obtained by the two methods agree and set the number of effective charges per channel to $z \simeq 13$. (*b*) Variance analysis of α_{1E}, $\alpha_{1E}\beta_{1a}$, and $\alpha_{1E}\beta_{2a}$ Ca^{2+} channels show that both the β_{1a} and β_{2a} subunits facilitate channel opening by shifting the activation curve to the left and that the β_{2a} subunit has the additional effect of increasing the limiting value of the open probability, Po_{max}. (*c*) The combination of variance analysis with the measurement of the gating charge (time integral of the gating current) gave different z values for α_{1E}, $\alpha_{1E}\beta_{1a}$, and $\alpha_{1E}\beta_{2a}$ Ca^{2+} channels. In our experimental conditions, the measured number of effective charges per channel is affected by the β subunit (z = 14.77 in α_{1E}, z = 15.13 in $\alpha_{1E}\beta_{1a}$ and z = 9.50 in $\alpha_{1E}\beta_{2a}$). (*d*) Limiting slope analysis of α_{1E}, $\alpha_{1E}\beta_{1b}$, $\alpha_{1E}\beta_{2a}$, $\alpha_{1A}\beta_{2a}$, and $\alpha_{1C}\beta_{2a}$ ($\alpha_{1C}\beta_{2a}$ and $\alpha_{1Cdel2}\beta_{2a}$) Ca^{2+} channels gave consistent results of $z = 8.6$.

Both methods used to determine z have inherent limitations and their validity is strictly dependent on the model of channel function. The variance analysis is

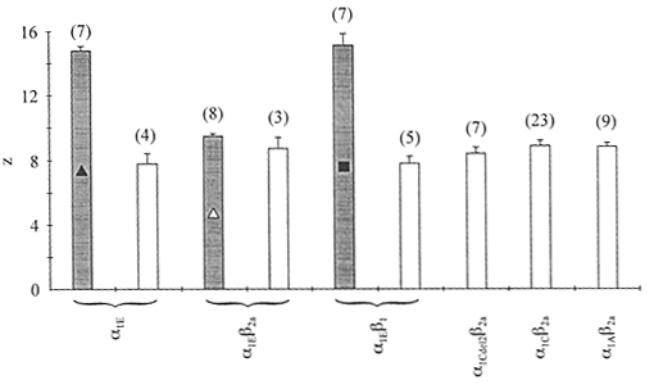

FIGURE 10. Summary plot of the results for various Ca^{2+} channels with or without different β subunits. The mean z values are plotted with their standard errors (SEM). The numbers in parentheses are the number of samples. The filled bars represent the results from the variance analysis, while the empty bars are the results from the limiting slope experiments. Symbols in the variance analysis bars refer to the plot in Fig. 8. The average value of z obtained with the limiting slope experiments is: $z = 8.58 \pm 0.18$.

valid only if all the channels open at least once during the pulse and thereby contribute to the noise fluctuations. Thus, we used large depolarizing pulses to maximize the probability of the final open state (O) in:

$$C\cdots C \leftrightarrow O\ . \qquad \text{(SCHEME I)}$$

If a fraction of channels do not open due to the existence of a parallel inactivated pathway with a kinetic model of the form:

$$\begin{array}{l} C\cdots C \leftrightarrow O \\ \updownarrow \\ I\cdots I \leftrightarrow I, \end{array} \qquad \text{(SCHEME II)}$$

N will be underestimated. If this fraction of silent channels carries charge movement, we will overestimate the Q_{max}/N ratio, leading to an erroneous higher z. This might be the case for some Ca^{2+} channels (Cavalié et al., 1983; Hess et al., 1984; Yue et al., 1990; Costantin et al., 1995) or for C-inactivated K^+ channels. The limiting slope method has an inherent experimental difficulty, since the single exponential approximation is valid only at very low Po (Almers, 1978). This method detects all the charges that move in the activation pathway to a final single open state, and it can be applied to a strictly sequential model or to a parallel model in which the parallel branches carry the same charge (see APPENDIX). If sufficiently small values of the Po cannot be reached (due to low resolution of the system), the error introduced by this analysis will consist of an underestimation of the number of effective charges per channel, thus diverging from the results of the variance analysis. In view of these facts, converging results obtained with the two methods give more reliability to the measurements, as well as to the predicted model.

The consistency between the results obtained for the *Shaker IR* K^+ channel by both variance analysis and limiting slope analysis, strongly suggests that all charge movement is coupled to pore opening. In agreement with previous measurements (Schoppa et al., 1992; Zagotta et al., 1994; Seoh et al., 1996), 13 effective charges are displaced during the closed-to-open transitions which occur in response to a depolarizing potential.

The different z values obtained with variance analysis of Ca^{2+} channels can be explained by the model in SCHEME II. Using that method, we found that α_{1E} and $\alpha_{1E}\beta_{1a}$ had a larger number of e_0 ($\simeq$15) than $\alpha_{1E}\beta_{2a}$ (9.50). On the other hand, using the limiting slope analysis, we measured an average of 8.6 e_0 for all the tested Ca^{2+} channel forms, including $\alpha_{1E}\beta_{2a}$. Thus, the z value for $\alpha_{1E}\beta_{2a}$ is about the same using both methods. Consistent with SCHEME II, where an increase in the population of the open state (increase in Po_{max}) would give a more accurate evaluation of z using the variance analysis method, coexpression with the β_{2a} subunit increased Po_{max} ($Po_{max\alpha 1E}$ = 0.56 and $Po_{max\alpha 1E\beta 1a}$ = 0.57 vs. $Po_{max\alpha 1E\beta 2a}$ = 0.78). Following SCHEME II, the increase in Po_{max} induced by β_{2a} should be associated with less frequent silent channels and an overall decrease of the null mode. In fact, β_{2a} increases the coupling efficiency (G_{max}/Q_{max} ratio; G_{max} is the limiting conductance) of α_{1E} Ca^{2+} channels (Olcese, R., personal communication). Moreover, since these changes occur without modifications in the activation time constant of the Ca^{2+} current, we can conclude that the current potentiation induced by β_{2a} is due to a smaller fraction of silent channels.

We conclude that the features of α_{1E} Ca^{2+} channels explored in this study follow SCHEME II and that the number of effective charges for all the tested Ca^{2+} channels (α_{1A}, α_{1E}, and α_{1C}) is $\sim$9 e_0.

APPENDIX

Limits of the Limiting Slope Analysis to Obtain z, the Effective Charge per Channel Coupled to Channel Opening

Sequential model. The LSA is valid only in a sequential model with one open state, where the transition rates are exponentially dependent on the voltage. We will assume that the rates are exponential functions of the energy (as predicted by Eyring theory), and that the energy is linearly dependent on the voltage. In the general case of $n + 1$ states,

$$C_0 \underset{\beta_0}{\overset{\alpha_0}{\rightleftarrows}} C_1 \underset{\beta_1}{\overset{\alpha_1}{\rightleftarrows}} C_2\cdots C_{n-1} \underset{\beta_{n-1}}{\overset{\alpha_{n-1}}{\rightleftarrows}} O, \qquad \text{(SCHEME III)}$$

where the rates of the transitions are:

$$\alpha_i = \alpha_i^0 e^{z_i \delta_i \frac{e_0 V}{kT}}$$

$$\beta_i = \beta_i^0 e^{-z_i (1-\delta_i) \frac{e_0 V}{kT}},$$

being α_i^0, β_i^0 the rates at zero voltage (s^{-1}), z_i the number of effective charges moved in the i-nth transition, δ_i the fraction of the field, V the membrane potential (V), e_0 the electronic charge (1.602×10^{-19} C), k the Boltzmann constant (1.38×10^{-23} J/K), and T the absolute temperature (K). The quantity δ_i, here defined as the fraction of the field, is not the same as x (see INTRODUCTION). The drawing represents a single energy barrier between two subsequent states. The fraction δ is the relative position of the peak of the energy barrier with respect to the initial and final states of the transition, while the fraction x represents the fraction of membrane that the energy barrier is spanning. Suppos-

ing $x = 1$, this would mean that the moving charge is crossing the whole lipid bilayer, and it is thus sensing all the potential difference between the intracellular and the extracellular sides.

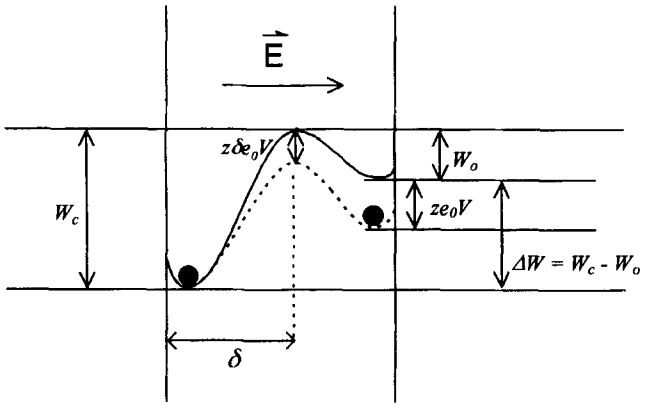

The steady state probability of the occurring of the open state O can be written as:

$$P_o = \frac{1}{1 + \sum_{j=0}^{n-1} \prod_{i=j}^{n-1} \frac{\beta_i}{\alpha_i}} = \frac{1}{1 + \sum_{j=0}^{n-1} \prod_{i=j}^{n-1} e^{-z_i (V - V_i) \frac{e_0}{kT}}}, \quad (4)$$

where V_i is the half-activation potential for the i-nth transition. V_i can be expressed as $V_i = V_i = \frac{\Delta W_i}{z_i e_0}$, where ΔW_i is the energy difference between the final and initial states of the transition. Thus, terms corresponding to noncharged transitions will contribute to the Po as functions of the only energy difference ΔW_i. In the limit for very negative potentials:

$$\lim_{V \to -\infty} P_o = \prod_{j=0}^{n-1} e^{\frac{e_0}{kT} z_j (V - V_j)} = e^{\frac{e_0}{kT} \sum_{j=0}^{n-1} z_j (V - V_j)} = \tilde{P}_o . \quad (5)$$

Thus, the total charge moved during all these transitions is:

$$z = \sum_{j=0}^{n-1} z_j = \frac{kT}{e_0} \frac{\mathrm{d}}{\mathrm{d}V} \ln \tilde{P}_o . \quad (6)$$

This approximation remains valid in the presence of noncharged steps in the activation pathway.

In a sequential model with two subsequent open states and two voltage-dependent transitions with charge z_1 and z_2,

$$C \leftrightarrow O_1 \leftrightarrow O_2 , \quad \text{(SCHEME IV)}$$

although the single exponential approximation for the G-V is still valid, the evaluated charge will be only z_1 carried along the first transition (C–O_1), whereas z_2 (O_1 – O_2) will not be detected through this method. Thus, as shown by Almers (1978), the LSA is only valid in the case of a sequential model with one open state in which the activation curve can be approximated with a mono-

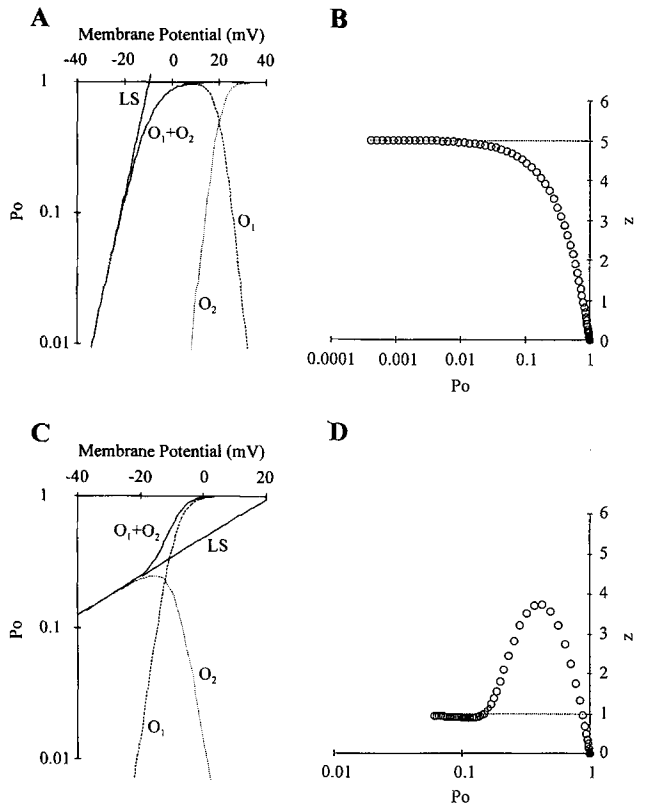

FIGURE 11. Simulation of *Po*-voltage curves and *z-Po* curves in a two branch parallel model (SCHEME V). (*A*) Semilog plot of *Po*-voltage curve calculated following Eq. 2. The parameters were: $z_1 = 5$, $V_1 = -10$ mV, $z_2 = 15$, $V_2 = 10$ mV. The two dashed lines are the probabilities of the two open states O_1 and O_2; the thick solid line is the sum of the two open probabilities. The limiting slope (LS, *thin solid line*) obtained by fitting to a single exponential gave: $z_{fit} = 4.95$, $V_{fit} = -9.7$ mV. (*B*) *z-Po* curve for the data in *A*. The horizontal dashed line corresponds to z_1. (*C*) Same plot as in *A*, but with $z_1 = 10$, $V_1 = -10$ mV, $z_2 = 1$, $V_2 = 10$ mV. The limiting monoexponential fit (LS) gave as results: $z_{fit} = 0.87$ and $V_{fit} = 20$ mV. (*D*) Calculated z values as in *B* (*circles*). The dashed line corresponds to z_2.

exponential function, with z being one of the parameters of the fit.

Parallel model. We will demonstrate that Eq. 6 cannot apply to a minimum parallel model. For example, we can consider a model with two open states connected to the same initial closed state, in which the two branches carry a different amount of charge z_1 and z_2:

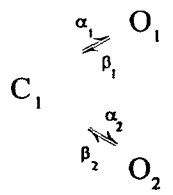

(SCHEME V)

In this case, the steady state probability of the open states $O_1 + O_2$ becomes:

$$P_o = \frac{1}{1 + e^{-z_1(V-V_1)\frac{e_0}{KT}}\left[1 + e^{z_2(V-V_2)\frac{e_0}{KT}}\right]} + \frac{1}{1 + e^{-z_2(V-V_2)\frac{e_0}{KT}}\left[1 + e^{z_1(V-V_1)\frac{e_0}{KT}}\right]}, \quad (7)$$

and, in the limit for very negative potentials the *Po* is:

$$\lim_{V\to-\infty} P_o = e^{z_1(V-V_1)\frac{e_0}{KT}} + e^{z_2(V-V_2)\frac{e_0}{KT}} = P_{o1} + P_{o2}. \quad (8)$$

In this case, the single exponential approximation is no longer valid. The transition with the lowest overall energy barrier at very negative voltages will be predominant, and the *z* value from a single exponential approximation will correspond to the charge carried along this branch.

In Fig. 11 we used Eq. 7 to calculate the *Po* values for SCHEME V. Two different sets of parameters have been used: in Fig. 11, *A* and *B*, the upper branch moves 5 e_0, with $V_1 = -10$ mV, and the lower branch moves 15 e_0, with $V_2 = +10$ mV. The main contribution to the open probability is given, for very negative potentials, by the transition C_1–O_1, and the limiting slope approximation (single exponential) gives as a result $z_{fit} = 4.95$. The graph in *B* shows the calculated values of *z(V)*. The simulation demonstrates that the charge carried by the lower branch ($z_2 = 15$) cannot be detected. Fig. 11, *C* and *D* are another simulation with the same half activation potentials (V_1 and V_2) as in Fig. 11, *A* and *B*, but with $z_1 = 10$ and $z_2 = 1$. In this case, the slope of the *Po-V* curve decreases at negative potentials below −20 mV, and the limiting slope approximation gives $z_{fit} = 0.91$. The graph in Fig. 11 *D* shows an increase in *z(V)* as the open probability decreases, but once O_2 becomes more populated than O_1, *z(V)* decreases again, and approximates z_2. A situation like the one simplified in SCHEME V can be applied to channels in which the movement of the charge is not yet complete when the channel is already fully opened. This is, for example the case of the Ca^{2+} activated K^+ channel *hslo* (Ottolia et al., 1996).

In conclusion, the LSA, in addition to its inherent limitation to obtain *Po* measurements at very negative potentials, (i.e., in the limit *Po*→0) is not adequate to obtain *z* in a parallel model of channel activation or in a sequential model with more than one open state.

We thank Ms. Jin for injection of *Xenopus laevis* oocytes.

This work was supported by grants from the National Institutes of Health grants AR38970 to E. Stefani; GM522203 to E. Stefani and L. Toro and AR43411 to L. Birnbaumer. N. Qin is the recipient of NIH National Research Service Award.

Original version received 22 April 1996 and accepted version received 13 June 1996.

REFERENCES

Almers, W. 1978. Gating currents and charge movements in excitatory membranes. *Rev. Physiol. Biochem. Pharmacol.* 82:96–190.

Almers, W., and C.M. Armstrong. 1980. Survival of K^+ permeability and gating currents in squid axons perfused with K^+-free media. *J. Gen. Physiol.* 75:61–78.

Begenisich, T., and C.F. Stevens. 1975. How many conductance states do potassium channels have. *Biophys. J.* 15:843–846.

Bezanilla, F., E. Perozo, D.M. Papazian, and E. Stefani. 1991. Molecular basis of gating charge immobilization in *Shaker* potassium channels. *Science (Wash. DC).* 254:679–683.

Bezanilla, F., and E. Stefani. 1994. Voltage dependent gating of ionic channels. *Ann. Rev. Biophys. Biochem. Chem.* 23:819–846.

Castellano, A., X. Wei, L. Birnbaumer, and E. Perez-Reyes. 1993*a*. Cloning and expression of a third calcium channel β subunit. *J. Biol. Chem.* 268:3450–3455.

Castellano, A., X. Wei, L. Birnbaumer, and E. Perez-Reyes. 1993*b*. Cloning and expression of a neuronal calcium channel β subunit. *J. Biol. Chem.* 268:12359–12366.

Catterall, W.A. 1988. Structure and function of voltage-sensitive ion channels. *Science (Wash. DC).* 242:50–61.

Cavalié, A., R. Ochi, D. Pelzer, and W. Trautwein. 1983. Elementary currents through Ca^{2+} channels in Guinea pig myocytes. *Pflüger Arch.* 398:284–297.

Conti, F., B. Hille, and W. Nonner. 1984. Non-stationary fluctuations of the potassium conductance at the Node of Ranvier of the frog. *J. Physiol. (Camb.).* 353:199–230.

Costantin, J.L., N. Qin, L. Birnbaumer, E. Stefani, and A. Neely. 1995. β subunit coexpression induces long channel openings in the α_{1C} cardiac calcium channel. *Biophys. J.* 68:A258. (Abstr.)

Greenblatt, R.E., Y. Blatt, and M. Montal. 1985. The structure of the voltage-sensitive sodium channel. Inferences derived from computer-aided analysis in the *Electrophorus electricus* channel primary structure. *FEBS Lett.* 193:125–134.

Guy, H.R., and P. Seetharamulu. 1986. Molecular model of the action potential sodium channel. *Proc. Natl. Acad. Sci. USA.* 83:508–512.

Heginbotham, L., and R. MacKinnon. 1993. Conduction properties of the cloned *Shaker* K^+ channel. *Biophys. J.* 65:2089–2096.

Hess, P., J.B. Lansman, and R.W. Tsien. 1984. Different modes of Ca channel gating behaviour favored by dihydropyridine Ca agonists and antagonists. *Nature (Lond.).* 311:538–544.

Hilgemann, D.W. 1989. Giant excised cardiac sarcolemmal membrane patches: sodium and sodium-calcium exchange currents. *Pflüger Arch.* 415:247–249.

Hirschberg, B., A. Rovner, M. Lieberman, and J. Patlak. 1995. Transfer of twelve charges is needed to open skeletal muscle Na^+ channels. *J. Gen. Physiol.* 106:1053–1068.

Hodgkin, A.L., and A.F. Huxley. 1952. A quantitative description of membrane current and its application to conduction and excitation in nerve. *J. Physiol. (Camb.).* 117:500–544.

Hoshi, T., W.N. Zagotta, and R.W. Aldrich. 1990. Biophysical and molecular mechanisms of *Shaker* potassium channel inactivation.

Science (Wash. DC). 250:533–538.

Kamb, A., J. Tweng-Drank, and M.A. Tanouye. 1988. Multiple products of the Drosophila *Shaker* gene may contribute to potassium channel diversity. *Neuron.* 1:421–430.

Larsson, H.P., O.S. Baker, D.S. Dhillon, and E.Y. Isacoff. 1996. Transmembrane movement of the *Shaker* K^+ channel S4. *Neuron.* 16:387–397.

Liman, E.R., P. Hess, F. Weaver, and G. Koren. 1991. Voltage-sensing residues in the S4 region of a mammalian K^+ channel. *Nature (Lond.).* 353:752–756.

Logothetis, D.E., S. Movahedi, C. Satler, K. Lindpaintner, and B. Nadal-Ginard. 1992. Incremental reductions of positive charge within the S4 region of a voltage-gated K^+ channel result in corresponding decreases in gating charge. *Neuron.* 8:531–540.

Mannuzzu, L.M., M.M. Moronne, and E.Y. Isacoff. 1996. Direct physical measure of conformational rearrangement underlying potassium channel gating. *Science (Wash. DC).* 271:213–216.

Neely, A., R. Olcese, P. Baldelli, X. Wei, L. Birnbaumer, and E. Stefani. 1995. Dual activation of the cardiac Ca^{2+} channel alpha 1C-subunit and its modulation by the beta-subunit. *Am. J. Physiol.* 268:C732–C740.

Neely, A., R. Olcese, X. Wei, L. Birnbaumer, and E. Stefani. 1994. Ca^{2+}-dependent inactivation of a cloned cardiac Ca^{2+} channel α_1 subunit (α_{1C}) expressed in *Xenopus* oocytes. *Biophys. J.* 66:1895–1903.

Neely, A., X. Wei, R. Olcese, L. Birnbaumer, and E. Stefani. 1993. Potentiation by the β subunit of the ratio of the ionic current to the charge movement in the cardiac calcium channel. *Science (Wash. DC).* 262:575–578.

Noda, M., S. Shimizu, T. Tanabe, T. Takai, T. Kayano, T. Ikeda, H. Takahashi, H. Nakayama, Y. Kanaoka, N. Minamino, et al. 1984. Primary structure of *Electrophorus electricus* sodium channel deduced from cDNA sequence. *Nature (Lond.).* 312:121–127.

Olcese, R., T. Schneider, A. Neely, X. Wei, J. Costantin, L. Birnbaumer, and E. Stefani. 1994. Tight coupling between charge movement and pore opening in type E calcium channel. *Biophys. J.* 66:A321. (Abstr.)

Olcese, R., L. Toro, F. Bezanilla, and E. Stefani. 1996. Correlation between charge movement and ionic current during C-Type inactivation in *Shaker IR* potassium channels. *Biophys. J.* 68:A32. (Abstr.)

Ottolia, M., F. Noceti, R. Olcese, M. Wallner, R. Latorre, E. Stefani, and L. Toro. 1996. Charge movement in a voltage and Ca^{2+} sensitive potassium channel (*hslo*). *Biophys. J.* 70:A193. (Abstr.)

Papazian, D.M., L.C. Timpe, Y.N. Jan, and L.Y. Jan. 1991. Alteration of voltage-dependence of *Shaker* potassium channel by mutations in the S4 sequence. *Nature (Lond.).* 349:305–310.

Perez-Reyes, E., A. Castellano, H.S. Kim, P. Bertrand, E. Baggstrom, A.E. Lacerda, X. Wei, and L. Birnbaumer. 1992. Cloning and expression of cardiac/brain β subunit of the L-type calcium channel. *J. Biol. Chem.* 267:1792–1797.

Perozo, E., R. MacKinnon, F. Bezanilla, and E. Stefani. 1993. Gating currents from a nonconducting mutant reveal open-closed conformations in *Shaker* K^+ channels. *Neuron.* 11:353–358.

Perozo, E., L. Santacruz-Toloza, E. Stefani, F. Bezanilla, and D.M. Papazian. 1994. S4 mutations alter gating currents of *Shaker* K channels. *Biophys. J.* 66:345–354.

Ruth, P., A. Rohrkasten, M. Biel, E. Bosse, S. Regulla, H.E. Meyer, V. Flockerzi, and F. Hofmann. 1989. Primary structure of the beta subunit of the DHP-sensitive calcium channel from skeletal muscle. *Science (Wash. DC).* 245:1115–1118.

Schneider, T., X. Wei, R. Olcese, J.L. Costantin, A. Neely, P. Palade, E. Perez-Reyes, N. Qin, J. Zhou, G.D. Crawford, et al. 1994. Molecular analysis and functional expression of the human type E neuronal Ca^{2+} channel alpha 1 subunit. *Receptors and Channels.* 2: 255–270.

Schoppa, N.E., K. McCormack, M.A. Tanouye, and F.J. Sigworth. 1992. The size of gating charge in wild-type and mutant *Shaker* potassium channels. *Science (Wash. DC).* 255:1712–1715.

Seoh, S.-A., D. Sigg, D.M. Papazian, and F. Bezanilla. 1996. Voltage-sensing residues in the S2 and S4 segments of the *Shaker* K^+ channel. *Neuron.* 16:1159–1167.

Sigg, D., E. Stefani, and F. Bezanilla. 1994. Gating current noise produced by elementary transitions in *Shaker* potassium channels. *Science (Wash. DC).* 264:578–582.

Sigworth, F.J. 1980. The variance of sodium current fluctuations at the node of ranvier. *J. Physiol. (Camb.).* 307:97–129.

Sigworth, F.J. 1994. Voltage gating of ion channels. *Quart. Rev. Biophys.* 27:1–40.

Singer, D., M. Biel, I. Lotan, V. Flockerzi, F. Hofmann, and N. Dascal. 1991. The roles of the subunits in the function of the calcium channel. *Science (Wash. DC).* 253:1553–1557.

Starr, T.V., W. Prystay, and T.P. Snutch. 1991. Primary structure of a calcium channel that is highly expressed in the rat cerebellum. *Proc. Natl. Acad. Sci. USA.* 88:5621–5625.

Stefani, E., L. Toro, E. Perozo, and F. Bezanilla. 1994. Gating of *Shaker* K^+ channels: I. Ionic and gating currents. *Biophys. J.* 66: 996–1010.

Stühmer, W., F. Conti, H. Suzuki, X. Wang, M. Noda, N. Yahagi, H. Kubo, and S. Numa. 1989. Structural parts involved in activation and inactivation of the sodium channel. *Nature (Lond.).* 339:597–603.

Tempel, B.L., D.M. Papazian, T.L. Schwarz, Y.N. Jan, and L.Y. Jan. 1987. Sequence of a probable potassium channel component encoded at *Shaker* locus of *Drosophila. Science (Wash. DC).* 237:770–775.

Wei, X., A. Neely, A.E. Lacerda, R. Olcese, E. Stefani, E. Perez-Reyes, and L. Birnbaumer. 1994*a*. Modification of Ca^{2+} channel activity by deletions at the carboxyl terminus of the cardiac α_1 subunit. *J. Biol. Chem.* 269:1635–1640.

Wei, X.Y., A. Neely, R. Olcese, E. Stefani, and L. Birnbaumer. 1994*b*. Gating and ionic currents from N-terminal deletion mutants of the cardiac Ca^{2+} channel α_1 subunit. *Biophys. J.* 66:A128. (Abstr.)

Wei, X., E. Perez-Reyes, A.E. Lacerda, G. Schuster, A.M. Brown, and L. Birnbaumer. 1991. Heterologous regulation of the cardiac Ca^{2+} channel α_1 subunit by skeletal muscle β and γ subunits. Implications for the structure of cardiac L-type Ca^{2+} channels. *J. Biol. Chem.* 266:21943–21947.

Williams, M.E., D.H. Feldman, A.F. McCue, R. Brenner, G. Velicelebi, S.B. Ellis, and M.M. Harpold. 1992. Structure and functional expression of α_1, α_2, and β subunits of a novel human neuronal calcium channel subtype. *Neuron.* 8:71–84.

Yang, N., A.L. George, Jr., and R. Horn. 1996. Molecular basis of charge movement in voltage-gated sodium channels. *Neuron.* 16: 113–122.

Yang, N., and R. Horn. 1995. Evidence for voltage-dependent S4 movement in sodium channels. *Neuron.* 15:213–218.

Yue, D.T., S. Herzig, and E. Marban. 1990. β-Adrenergic stimulation of calcium channels occurs by potentiation of high-activity gating modes. *Proc. Natl. Acad. Sci. USA.* 87:753–757.

Zagotta, W.N., T. Hoshi, J. Dittman, and R.W. Aldrich. 1994. *Shaker* potassium channel gating. II: Transitions in the activation pathway. *J. Gen. Physiol.* 103:279–319.

Zampighi, G.A., M. Kreman, K.J. Boorer, D.D. Loo, F. Bezanilla, G. Chandy, J.E. Hall, and E.M. Wright. 1995. A method for determining the unitary functional capacity of cloned channels and transporters expressed in *Xenopus laevis* oocytes. *J. Membr. Biol.* 148:65–78.